PROCEEDINGS A

royalsocietypublishing.org/journal/rspa

Research

Cite this article: Grassia P, Torres-Ulloa C, Hernández-Montelongo J. 2024 A cluster of *N*-bubbles driven along a channel at high imposed driving pressure: film orientations and bubble pressures. *Proc. R. Soc. A* **480**: 20230722.
https://doi.org/10.1098/rspa.2023.0722

Received: 29 September 2023
Accepted: 10 May 2024

Subject Areas:
applied mathematics, mathematical modelling, fluid mechanics

Keywords:
viscous froth model, foam flow in channels, foam film orientations, bubble pressures, staircase structure, mathematical modelling

Author for correspondence:
Paul Grassia
e-mail: p.s.grassia@tue.nl

Electronic supplementary material is available online at https://doi.org/10.6084/m9.figshare.c.7315701.

THE ROYAL SOCIETY PUBLISHING

A cluster of *N*-bubbles driven along a channel at high imposed driving pressure: film orientations and bubble pressures

Paul Grassia[1,2], Carlos Torres-Ulloa[3,4] and Jacobo Hernández-Montelongo[4]

[1]Department of Mechanical Engineering, TU Eindhoven, Groene Loper 3, 5612 AE Eindhoven, The Netherlands
[2]Department of Chemical and Process Engineering, University of Strathclyde, James Weir Building, 75 Montrose Street, Glasgow G1 1XJ, UK
[3]Centro de Investigación, Innovación y Creación (CIIC), and
[4]Departamento de Ciencias Matemáticas y Físicas, Facultad de Ingeniería, Universidad Católica de Temuco, Rudecindo Ortega 03694, Temuco, Chile

PG, 0000-0001-5236-1850

A cluster of N bubbles (with N odd) arranged in a channel in a zigzag staircase configuration is modelled. A limiting case is considered in which the staircase is set into motion by the application of a high driving pressure. In this limit, foam films between bubbles are predicted to become asymptotically flat. Angles at which these flat films are oriented and also bubble pressures are then determined. For N bubbles, the film orientations and bubble pressures differ from predictions for a staircase in the limit of an infinite number of bubbles. Differences are significant towards the downstream end of a staircase, but decay moving upstream. However, the decay is gradual. Hence, a very large N is needed for a finite staircase to align its film orientations towards its upstream end with the orientations in an infinite staircase.

1. Introduction

There are several scenarios in daily life, in engineering and also in the environment, in which foam films flow along narrow channels. These include foam within dishwashing sponges [1], foam microfluidics [2], foam-based medical treatments [3,4], foam improved/enhanced oil recovery [5–9], foam-based carbon capture [10,11] and foam-based soil/aquifer remediation [12–26]. One reason that foam is used in applications like these is that it has surprisingly low mobility as it moves along channels [27,28]: a multi-phase system containing foam films is more difficult to drive along a channel than a single-phase fluid would be [29–33]. This then means that low-mobility foam can displace other more mobile fluids from channels [5,8,20,21]. Ability to predict the mobility of foam in channels is therefore of interest.

However, the mobility of foam in channels is sensitive to how foam is structured. Indeed, mobility depends upon the manner in which foam films and the bubbles separating them are arranged spatially [34]. This, in turn, has generated interest in studying flowing foams with the bubbles and the films separating them arranged within channels in rather specific ways [2,35–40]. Often foam flow applications seek to increase flow rate (i.e. to increase throughput) by increasing an imposed driving pressure. Increasing driving pressure can cause flowing foam films to change their shape [41,42] (details of resulting film shapes will be reviewed in §2). Moreover, sufficiently high driving pressures might cause bubbles to rearrange spatially within channels, losing contact with neighbouring bubbles and/or forming new contacts [2,35,37,38,41,43–47].

As has been mentioned, studies are often focused on bubbles arranged spatially in certain ways and the mobility associated with such arrangements [34,39]. If bubbles rearrange, however, the original arrangement and the mobility determined specifically for it cease to be relevant. In view of the above, there is interest in studying systems that can *resist* rearrangements even out to very high flow rates, corresponding to driving the system at very high imposed pressures, but with known mobility. Modelling-based studies have predicted that such situations can exist [42,45–47] provided a bubble size is chosen compatible with channel size (again details of how bubbles and films might be configured will be discussed in §2).

A widely studied case in this context, owing to the richness of behaviour that it admits, is a three-bubble structure [45–47]: two of the bubbles are placed towards one side of a channel, and the third bubble is placed towards the other side of it. In this three-bubble case, if the given bubble arrangement is to remain viable even out to high imposed driving pressures, it turns out that there are very specific constraints upon how foam films must be oriented [45] (a sketch of the three-bubble structure and details of the film orientations are given in figure 1).

Applications involving foam flow in channels need not however involve as few as three bubbles being present. Instead, looking along various paths though a porous medium for instance [28], one could encounter a train of many bubbles [2]. In view of that, the novel contribution of the present work is to extend the aforementioned modelling-based studies [45–47] so as to consider the orientations of fast flowing foam films in a channel in a situation when many bubbles are present. Although film orientations in the limit of an infinite number of bubbles can be found very straightforwardly [42], a surprising finding to be presented here is that the case of a large but finite number of bubbles approaches that limit only rather gradually.

The remainder of this work is laid out as follows. Section 2 describes background material in order to set the context better, and explains how the novel contribution of the present work fits within that context. Section 3 describes the general details of the mathematical model. Section 4 then explains how to formulate the model to treat the specific novel questions to be addressed here. After that §5 analyses the model in the case of many bubbles. Section 6 then presents results and §7 gives conclusions and an outlook. The appendix provides some electronic supplementary material, S1–S6.

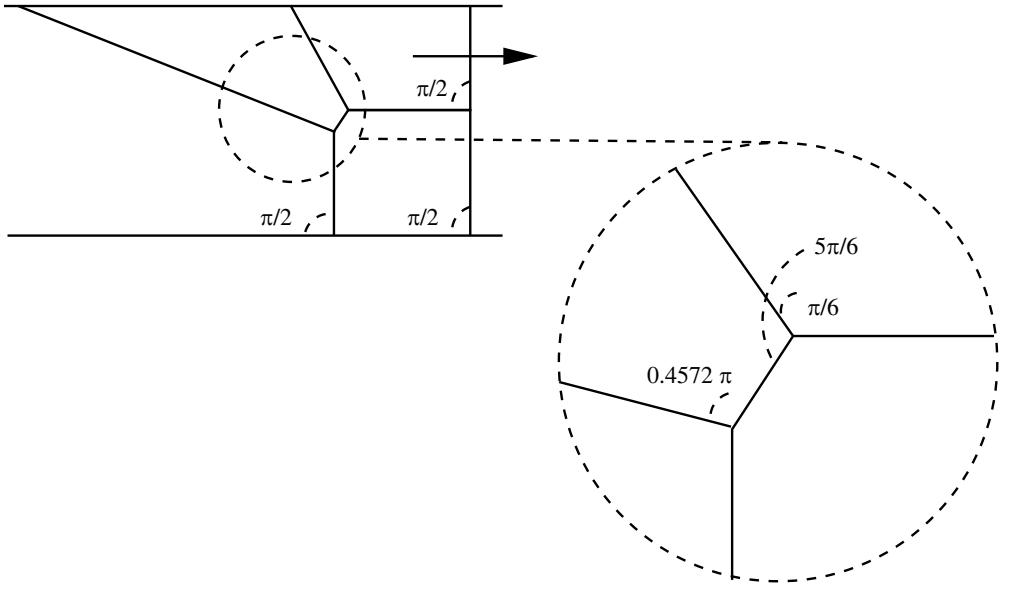

Figure 1. Configuration of a three-bubble staircase driven from left to right due to a large imposed pressure. The orientation angles of various films (all angles being measured relative to the vertical) are shown. There are constraints on angles at which films meet each other and on angles at which films meet channel walls: as will be explained, these constraints can still be satisfied even despite appearances to the contrary.

2. Background and novel contribution

This section begins by reviewing background material setting the context of this study (§2a). It then goes on to describe the novel contribution to be made here (§2b).

(a) Context and background

A detailed discussion of the background to this work can be found in the literature [2,36,41–48] and (for the benefit of readers unfamiliar with that literature) also in §S1 in the electronic supplementary material. However, key ideas are highlighted in what follows.

The context for the present work is flow of bubbles in a Hele–Shaw cell [49] (see e.g. figure S1*a* in the electronic supplementary material). The cell consists of two closely spaced plates, with a narrow gap between them. Sidewalls define the width of the cell (which is assumed much greater than the gap thickness), while the length of the cell is in turn much larger than the width. Bubbles are assumed to be stacked in a so-called zigzag staircase arrangement [2,36], two bubbles across the cell width, multiple bubbles along the cell length but just a single bubble across the narrow gap thickness. Figure S1*b* in the electronic supplementary material is a view of the staircase from above the cell, so the bubbles appear to be two-dimensional objects. What are actually sidewalls of the cell appear in the two-dimensional view to be upper and lower channel walls (and will be referred to as such).

The staircase structures studied here are comprised [50] of the bubbles themselves, films between bubbles and also vertices at which three films meet. The foam is considered to be dry, so films can be treated as one-dimensional lines (or more generally curves) and vertices can be treated as points. In figure S1*b*, films meet the upper and lower channel walls at right angles (assuming a narrow Hele–Shaw gap thickness [42,51]), whereas at vertices they meet at $2\pi/3$ angles according to the so-called Plateau's Laws [52,53]. Bubbles can be set into motion (from left to right in the electronic supplementary material, figure S1) by the action of an imposed driving pressure.

The structure sketched in the electronic supplementary material, figure S1*b* (likewise the electronic supplementary material, figure S2) is assumed to be a section of a so-called infinite staircase, which extends arbitrarily far along the channel in both directions. It turns out that this can propagate along the channel without deforming at all [42], at least in the limit considered here (Hele–Shaw gap thickness much smaller than the channel width [42,51]).

In a moving staircase, there must be a pressure difference from bubble to bubble, with bubbles upstream having higher pressure than those downstream. However, this pressure difference is balanced by drag on the moving films between the bubbles. Films that are oriented obliquely experience less drag than those that are oriented at right angles to channel walls [34]. Indeed, in the electronic supplementary material, figure S1*b*, the zigzag films turn out to be oriented so as to have exactly half the drag (per unit length of film) as the films that connect to the channel walls. Hence, the pressure drop across each zigzag film is likewise half as large as across the films connecting to the channel walls.

Even though studying the infinite staircase is instructive, in real systems, we only ever have a finite number of bubbles flowing along. It is then of interest to know how many bubbles might be necessary to approach infinite staircase behaviour. This has led in turn to studies on truncated staircases rather than infinite ones [41,43–48]. Typically, truncated staircases with odd numbers of bubbles are of interest [41,45,46]. This is because they exhibit topological asymmetry [47], i.e. they have more bubbles (and consequently more films) on one side of the channel than the other. Since drag is tied to moving foam films, this means that the side which has more films also potentially experiences more drag.

Unlike what happens with the infinite staircase, having drag on the films causes a truncated staircase to deform. If the number of bubbles is odd, then the bubbles on the side of the channel with more films and hence typically more drag, tend to lag behind bubbles on the other side. If the system is driven at sufficiently high pressure, bubbles can potentially lag so far behind that they separate off from the rest of the structure [41,45–47]. In other words, bubbles rearrange and exchange neighbours in a process known as a topological transformation or *T*1 transformation.

After a *T*1, typically individual bubbles that have lagged behind and separated off from the rest of the structure remain fixed on a channel wall without propagating any further [41,47]. The rest of the structure however can continue to propagate along the channel. The part of the structure that continues propagating along however has a different mobility from the original structure prior to the *T*1 (mobility here being defined as the ratio between imposed driving pressure and propagation velocity) [47]. Given the important role of mobility (as already discussed in the Introduction) in governing applications involving foam flow along channels, knowing about *T*1 transformations is likewise important.

One drastically truncated staircase system studied in the literature is the so-called simple lens [41,43,44,48], consisting of a single bubble plus an additional film (see figure S3 in the electronic supplementary material). If driven with high enough pressure, the simple lens always breaks via a *T*1 [41]. High imposed pressure in this context means high relative to a typical capillary pressure scale (the ratio between film tension and width of the Hele–Shaw channel). This is still much smaller than atmospheric pressure, so bubbles remain incompressible. In two dimensions as studied here, this implies bubbles conserve area even as they deform and undergo *T*1 transformations.

There is a contrast between an infinite staircase that does not break or even deform when it is driven along a channel, whereas a simple lens always deforms and, at high enough imposed pressure, eventually breaks. In an effort to find a bridge between the behaviours of the infinite staircase and simple lens, a three-bubble system has been studied [45–47]. This consists of two bubbles attached to the upper channel wall and one bubble attached to the lower channel wall.

The three-bubble system is found often to break up at high imposed pressure, but occasionally it survives even in a high-pressure limit [45,46]. Whether the three-bubble system breaks up or survives, depends primarily on the size of the bubbles, measured in two dimensions by bubble areas that are conserved as has been mentioned (details can be found in the electronic supplementary material, section S1c).

What happens for those three-bubble systems that resist breaking is that, as pressures are imposed, first of all the structure deforms. However, eventually a configuration is reached after which there is no further deformation even as the pressure increases further. This configuration is then termed a geometrically invariant state [45]. Further increases in pressure merely change the velocity at which the structure propagates along (changing also the drag on the films). In spite of that, the geometry (represented by the shape of each bubble) does not continue to change.

It is possible to compute what the structure of the geometrically invariant state must be. More precisely, we can identify necessary conditions for such a state to exist, and then determine the resulting structure provided those necessary conditions are met [45]. A sketch of the structure thereby obtained is shown in figure 1. In this figure, films are flat and they are also constrained to be oriented at very particular angles [45]. There are two films connected to the lower channel wall which is oriented at right angles to the wall. Three films are connected to the upper channel wall, one at a right angle to the wall, while two of them are oriented obliquely. As already mentioned, drag on oblique films is less than that on films oriented at right angles to the wall [34]. That then compensates for having more films on one channel wall than the other.

Figure 1, however, also presents an apparent paradox. It has been mentioned already that films should meet channel walls at right angles, but in figure 1 that appears to be violated for two of the films at the upper channel wall. Likewise, films should also meet at $2\pi/3$ angles at threefold vertices [52,53], but again that appears to be violated for the downstream most vertex, and (consulting the zoomed view in figure 1) for the upstream most vertex also. We emphasize though that these are only apparent violations. In fact, there can be very sharply curved regions in the neighbourhood of walls and/or vertices that restore the correct angles [41,45]. We will discuss later on more about how this situation can come about. However, because the sharply curved regions can be shown to be very limited in extent [41,45], we do not need to resolve them in figure 1, nor even to account for them in order to construct the geometrically invariant state.

Indeed given just the orientation angles already shown in figure 1, we can attempt to construct a three-bubble staircase with bubbles of a given target area (see section S1d in the electronic supplementary material). If bubble areas are chosen too small, it turns out that constructing the state in figure 1 is not possible. For sufficiently large bubbles though (area on the order of the square of a channel width) a geometrically invariant state can feasibly be constructed [45].

Meeting necessary conditions on bubble areas to permit construction of a geometrically invariant state is not however a guarantee that the state itself will be realized when the three-bubble system is evolved dynamically. In fact, for the three-bubble system, it turns out that the geometrically invariant state is achieved dynamically for just a small set of all the bubble areas for which it can in principle exist [45,46]. Indeed, for many choices of bubble areas, often the three-bubble system breaks via a topological transformation even before managing to reach the geometrically invariant state. Despite this, being able to construct the geometrically invariant state in the first place remains useful. Once the state itself is identified, small perturbations can be imposed upon it and stability to those perturbations can be tested [46].

To summarize, the three-bubble system [45–47] deforms and often breaks via a topological transformation when subject to high imposed pressure. Sometimes however it deforms only up to a certain point, then ceases deforming any further and avoids breaking. The three-bubble system is therefore a bridge between the behaviours of the simple lens (which always deforms and breaks at sufficiently high imposed pressure) [41] and the infinite staircase (which never breaks nor even deforms). Although a great deal is therefore known about the three-bubble system, open questions still remain for more general staircase structures as we now discuss.

(b) Open questions and novel contribution

One open question that the present work begins to address is whether by adding more bubbles (over and above the three bubbles considered in previous work [45–47]), it might somehow be possible to make a staircase with a finite number N of bubbles starting to behave more like an infinite staircase structure. Indeed, a related open question for increasing N is whether over a

comparatively wide set of bubble sizes (measured here by bubble areas), the actual behaviour might attain a geometrically invariant state at high imposed pressures: by contrast, the three-bubble structure only admitted a geometrically invariant state in practice over a narrow set of areas [45,46]. Before we can answer this question though, it is necessary to know how the geometrically invariant state itself is configured for N bubbles. That in itself is a non-trivial question, and so is the specific question focused upon here.

Moreover, for N bubbles, just as was the case for three bubbles, there are two separate aspects to determining the geometrically invariant state. One is determining the set of film orientations that flat films within the geometrically invariant state must have: this can be determined independently of any bubble areas. This other is, given those orientations, determining flat films with the required film lengths, such that bubbles are constructed enclosing the correct areas. The novel contribution of the present work focuses just on the question of film orientations in an N-bubble structure, with determination of film lengths deferred to further work.

That said, if the geometry of a system with a large but finite number of bubbles is to approach anything like the geometry of an infinite staircase, then a necessary condition is that the orientations must match. For three bubbles of course (see the discussion of figure 1 earlier on) matching of film orientation angles with the corresponding orientation angles for an infinite staircase (see the electronic supplementary material, figure S1*b*) is poor [45]. For N bubbles, however, it is an open question whether or not a reasonable match could still be obtained overall, even though orientations fail to match over certain parts of the structure. For instance, matching might be poor towards one or other end of a large but finite staircase, but still be reasonable over much of the staircase (away from the ends say). As we will see, matching of film orientation angles turns out to be poor towards the downstream end of a large but finite staircase, but improves moving upstream, albeit the improvement tends to be only gradual as the number of bubbles increases.

In summary, a reason given in the literature for studying the three-bubble structure [45–47] is that its behaviour forms a bridge between the simple lens and infinite staircase. However, another important justification for studying the three-bubble structure is that it can provide intuition necessary for understanding structures with large but finite N. This intuition is then what is exploited here as we take a step towards understanding large but finite N structures. The various open questions mentioned above will be addressed using a model to be presented next.

3. Model

As already alluded to (see figure S1*a* in the electronic supplementary material), the system modelled here is a Hele–Shaw channel between confining plates, but viewed from above as if it were a two-dimensional structure (see e.g. figure 1 or figure S1*b*). The model of choice is the so-called viscous froth model [2,36], which is suitable for describing foams in the dry limit as considered here. Note that this model contains a viscous drag term: including a drag term like that is essential in order to predict behaviours at high driving pressures that differ from behaviours at low driving pressures. It is the high driving pressure limit in particular that interests us here, and some readers already familiar with the viscous froth model may wish to skip directly to §4 in which that particular limit is discussed. For the benefit of readers who are less familiar with the model however, information is provided in §3a–c.

(a) Viscous froth governing equation

As has been mentioned, various components can be included in models for foam structures (bubbles, films, vertices, Plateau borders and such like [50]). In the viscous froth model, however, the basic structural unit is an element of foam film [36]. Films are constructed by connecting these structural units (film elements) together. The viscous drag term represents drag associated with moving the film element relative to the confining plates of the Hele–Shaw cell.

The governing equation for each film element is [36,41]

$$\zeta v_*|\cos\phi| = \Delta p_* - 2\sigma\kappa_*. \tag{3.1}$$

Here, ζ is a drag coefficient, v_* is an apparent steady migration velocity along the plates, $\cos\phi$ is the cosine of a film orientation angle (the angle being measured relative to the vertical in the two-dimensional view in figure 1, which physically means relative to the direction across the channel width in the electronic supplementary material, figure S1*a*). Note that $v_*|\cos\phi|$ is a velocity normal to a film element, and can be less than the apparent velocity v_*. Meanwhile, Δp_* is a pressure difference across a film, σ is a surface tension, 2σ is a film tension (films have two surfaces) and κ_* is a film curvature.

Film curvature (see also figure S4*a*,*b* in the electronic supplementary material for some specific examples of curved films) is measured here solely in the direction along the two-dimensional film, i.e. across the width of the Hele–Shaw channel. This does not however mean that curvature is absent in the direction normal to the two-dimensional plane of interest here, i.e. in the direction across the thickness of the gap of the Hele–Shaw cell (reiterating also that this gap thickness is assumed much smaller than the width across the Hele–Shaw channel). As is explained in the literature [51], curvature normal to the plane causes film elements to bulge across the Hele–Shaw gap thickness (albeit not visible in a two-dimensional view). Nevertheless, the amount that film elements bulge across the gap thickness determines also the angle through which the films turn when moving across that thickness [51]. Moreover, as these bulging films meet the plates that confine the gap, those films swell into Plateau borders. The angle through which the bulging films have turned across the gap thickness then manifests itself in the amount of drag needed to move the Plateau borders relative to the confining plates [51]. This then is why equation (3.1) includes curvature only in the direction along the two-dimensional film element, but also has a drag term (in lieu of curvature across the gap thickness).

For films set into motion by an imposed pressure, we adopt sign conventions such that v_* is positive from left to right, Δp_* is positive from left to right, and κ_* is positive if a film is convex when seen from downstream and κ_* is negative if a film is concave when seen from downstream. The convention for ϕ is that it is measured anticlockwise from the vertical in figure 1, which also shows some angles explicitly. As already mentioned, the vertical in this two-dimensional view is actually the direction across the width of the Hele–Shaw channel. Values of ϕ can vary between 0 and π, but note that equation (3.1) involves $|\cos\phi|$ rather than simply $\cos\phi$.

(b) Governing equation in dimensionless form

We now proceed to make the governing equation dimensionless. A Hele–Shaw cell of width L is assumed. Distances are made dimensionless with respect to L. Curvatures are made dimensionless with respect to L^{-1}. Pressures are made dimensionless with respect to $2\sigma/L$. Velocities are made dimensionless with respect to $2\sigma/(L\zeta)$.

To give a sense of scale, we suppose that L is around 9×10^{-3} m, σ is around $27\times10^{-3}\,\mathrm{N\,m^{-1}}$ and ζ is around $290\,\mathrm{kg\,m^{-2}\,s^{-1}}$. There is some uncertainty in the value of ζ, which in principle could be sensitive to velocity and also to gap thickness [41], but we use the aforementioned value in line with estimates in prior work [41,47]. Note that one unit of velocity is now $0.020\,\mathrm{m\,s^{-1}}$ and one unit of pressure is now 6 Pa. The unit of pressure in particular is much less than atmospheric pressure, which implies that gas in bubbles is not compressed. As already mentioned this means that (in two dimensions) bubble areas are fixed even when bubble shapes deform: the present work however focuses just on film orientations, rather than upon bubble areas.

Using the above-mentioned scales, a dimensionless equation is now obtained

$$v|\cos\phi| = \Delta p - \kappa, \tag{3.2}$$

where v is dimensionless migration velocity, Δp is dimensionless pressure difference and κ is dimensionless curvature.

(c) Approaching the high velocity (i.e. high driving pressure) limit

In the present work, we are interested in limits in which Δp and v are large dimensionless values: Δp is uniform along any given film, whereas v is uniform over the entire structure, provided the structure is propagating steadily along. It is known that [41,42,45,46], in the limit of large driving pressures (equivalently in the limit of high migration velocities), films become 'asymptotically flat'. In other words, films are flat over most of their length, except for a region of sharp curvature near one or other end. In the three-bubble structure for example, values of pressure drop per film Δp and/or velocity v of the order of around 40 dimensionless units were found to be more than adequate to reach a flat film state, assuming the structure did not break prior to reaching that state [45,46].

Intuitively, the fact that films must be asymptotically flat can be deduced from equation (3.2). According to that equation, curvature κ is the difference between Δp and $v|\cos\phi|$. In the limit of interest, Δp and v are large dimensionless quantities, but with Δp no larger than v. There can be only one orientation angle at which Δp and $v|\cos\phi|$ match perfectly. Only at that particular orientation angle can the film curvature vanish. However, if the film is required to turn through a significant angle along its length [41] (in order to meet boundary conditions say), then there must be at least some parts of the film upon which there is a large imbalance between Δp and $v|\cos\phi|$, i.e. there must be at last some parts of the film upon which the curvature is large. The angle through which a film turns is (by definition) the integral of curvature along the film length. It then follows that large curvatures can only be sustained over small distances. Moreover, increasing the values of Δp and v decreases the distance over which large curvatures are sustained. As has been mentioned, the remainder of the film becomes asymptotically flat [42]. That then prevents the film turning through too great an angle.

The notion of having sharp curvature towards the end of a film is entirely consistent with the mathematical structure of equation (3.2). In this equation, the curvature κ involves a second derivative of the film coordinates with respect to arc length along a film [41]. The term in $\cos\phi$ however can be expressed in terms of a film tangent, which is only a first derivative of the film coordinate. In the limit of large Δp and large v, the weakest term in the equation is the one involving the highest spatial derivative. In a scenario like that [54], we can neglect this term over much of the film, but we still do need to account for it somewhere within a boundary layer [41]. It turns out that, regardless of whether a film is convex or concave, the region of sharp curvature is always located towards the upstream end of any individual film [41,42]. The reasons why the upstream end is selected are explained in section S2 in the electronic supplementary material.

Thus far via equation (3.2), we have analysed just elements upon a single film. However, our ultimate interest is in a staircase structure of N bubbles (typically with N odd to impose topological asymmetry). We are therefore interested not merely in upstream and downstream ends of individual films, but also in films towards the upstream and downstream ends of the staircase as a whole. When multiple bubbles and hence multiple films are involved, it is necessary to consider the angles at which films meet each other and also the angles at which films meet channel walls. In other words, we need to impose boundary conditions on film orientations for the entire set of films throughout the staircase structure.

As already mentioned, according to Plateau's Laws [52,53], films should meet each other at threefold vertices at angles of $\frac{2\pi}{3}$. Likewise, films should meet channel walls at right angles, at least in the limit to be assumed here whereby the gap thickness between Hele–Shaw plates is much less than the channel width of the Hele–Shaw cell. It is possible to generalize this away from right angles at walls in the case when gap thickness starts to become significant relative to channel width [42,51,55,56], but we will not consider such complications here.

Note however the flat film states to be considered here are exceptions to the above-mentioned rules on meeting angles. The rules are always satisfied at the downstream end of any given film. However, because films can curve sharply at their upstream ends [41,42], they can *appear* to violate the above-mentioned rules at their upstream ends (see e.g. figure 1). The rules are in fact satisfied even at the upstream ends owing to sharp curvature, but if we seek to determine only the flat

sections of films (as will be the case here), there is an apparent violation. In effect then, curvature is only relevant within boundary layers [54] near the upstream ends of films [41]. However, all that we need to find in the present work, are just outer solutions for each film away from those boundary layers.

To summarize, in the limit of arbitrarily high driving pressures (as will be considered here), any curvature is arbitrarily sharp, and is confined to an arbitrarily small region at the film's upstream end. The remainder of the film once it has flattened out, cannot change geometrically any further, so the state is now termed 'geometrically invariant' as alluded to earlier. In this limit, changing the driving pressure changes only the migration velocity (with pressure and velocity now being proportional), while the geometry remains unaffected.

Computing the resulting flat film geometry involves as a first step, computing film orientations subject to constraints at the ends of films, where either threefold vertices leading to other films or else channel walls are encountered. As has been mentioned, those constraints are strictly enforced at the downstream ends of films, but can appear to be violated at upstream ends. Determining the resulting film orientations for N bubbles is the novel contribution here, and is what we proceed to do next.

4. N-bubble staircase subject to high driving pressures

In this section, we first consider equations governing a geometrically invariant or flat film state that arises for high driving pressures (§4a). We then explain how to enumerate topology for an N-bubble staircase (§4b). After that §4c–g indicate how to formulate (and solve) equations for film orientations assuming an N-bubble staircase in a flat film state: this is done by analysing the staircase in various pieces.

(a) Flat film state

Here, we derive equations governing film orientations (specifically film orientation angles) and also bubble pressures assuming throughout flat films. As we will see, film orientations and bubble pressures are inseparable, so must be obtained together.

Our starting point is the dimensionless viscous froth equation for a flat film state

$$\Delta p = v|\cos\phi|, \tag{4.1}$$

where (as already mentioned) Δp is a driving pressure difference, v is a migration velocity along the channel and ϕ is an orientation angle (of the film tangent relative to the vertical). Mathematically, this model is equivalent to a model in the literature called pressure-driven growth [57], with the exception that pressure-driven growth typically incorporates an additional hydrostatic pressure term, which is not relevant here.

According to equation (4.1), if the film tangent deviates from vertical, then a given migration velocity can be sustained with less driving pressure than for a vertical film. For a specified orientation angle though, pressure and velocity are clearly proportional. Note also that the migration velocity v along the channel is uniform over the entire structure [41], but the pressure p varies from bubble to bubble. It is then convenient to define normalized pressures as

$$P = \frac{p}{v}, \tag{4.2}$$

in which case we have a normalized pressure difference across any given film

$$\Delta P = |\cos\phi|. \tag{4.3}$$

In what follows, we will work primarily in terms of normalized pressures P, not the original pressures p. For brevity therefore, we will refer simply to 'pressure'.

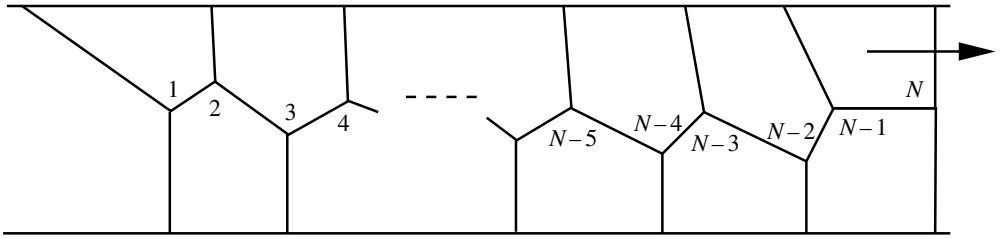

Figure 2. View of the topology and also (schematically) the expected film orientations for an N-bubble staircase (with N odd) moving from left to right. The numbers indicated here label both bubbles and vertices. Film orientations shown here are schematic, as determining what the orientations actually are is the purpose of the present work.

(b) Enumerating the staircase topology

We now apply equation (4.3) to the staircase topology. This consists of N bubbles in total, where N is odd. Figure 2 shows a sketch of what we expect the topology to be (generalizing figure 1 in an intuitive fashion) and also schematically what we expect the film orientations to be (to be discussed shortly). Bubbles are numbered from left to right, and are assigned an index J. Odd-numbered bubbles are attached to the upper channel wall, and even-numbered bubbles are attached to the lower channel wall. The pressure of bubble J is denoted P_J.

In addition to there being N bubbles, there are also N vertices. Vertices are again numbered from left to right, and are assigned an index J. Note that odd-numbered vertices are lower down within figure 2 than even-numbered vertices are.

Bubbles $J-1$, J and $J+1$ meet at vertex J. This is also true for vertex N at the far downstream end of the staircase, and for vertex 1 at the far upstream end of the staircase, provided we define, respectively, bubble $N+1$ to be the outside of the structure at the downstream end, and bubble 0 to be the outside of the structure at the upstream end.

Three films also meet at each vertex. Films are most conveniently labelled by the pair of bubbles which they separate. Indeed, film $J-1,J$, film $J-1,J+1$ and film $J,J+1$ all meet at vertex J. These have orientation angles $\phi_{J-1,J}$, $\phi_{J-1,J+1}$ and $\phi_{J,J+1}$, these angles being measured relative to the vertical. These film orientations, which are merely shown in a schematic format within figure 2, are what we aim to determine here. Note also that film $J-1,J$, as well as separating bubbles $J-1$ and J, also joins vertex $J-1$ with vertex J. An analogous statement applies to film $J,J+1$, which joins vertex J with vertex $J+1$. As well as the films zigzagging from vertex to vertex ($N-1$ such films in total), there are also films connected to the lower channel wall (one such film per odd-numbered vertex, $(N+1)/2$ in total). In addition, there are $(N+3)/2$ films connected to the upper channel wall (one per even-numbered vertex, plus an extra film at the first vertex and at the last vertex).

Note an important feature of figure 2 as drawn (also evident in figure 1 [45]). Films connecting to the lower channel wall are drawn oriented at right angles to the wall (implying that they are configured analogously to figure S4*a* in the electronic supplementary material). Films connecting to the upper channel wall (with the exception of the downstream most of them) are drawn oriented obliquely (implying that are configured analogously to figure S4*b* in the electronic supplementary material). The alternative (oblique films connected to the lower channel wall, right angle films connected to the upper channel wall) is not allowed. This follows from equation (4.3). If we sum the ΔP values in equation (4.3) crossing all the $(N+1)/2$ films connected to the lower channel wall, we must have the same result as if we sum the ΔP values crossing all the $(N+3)/2$ films connected to the upper channel wall. Since there is one extra film included in the sum in the case of the upper channel wall, the individual $\cos\phi$ terms must be smaller for the films connected to the upper channel wall.

Of course, films in figure 2 (as in figure 1) are drawn as being flat. As already mentioned (see §3c), these are outer solutions that neglect sharply curved regions at upstream ends of films.

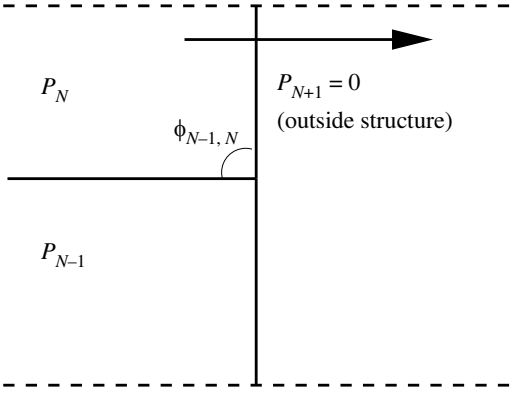

Figure 3. Configuration at the downstream end of the staircase. Motion is from left to right.

For films connecting to the lower channel wall (and also for the downstream most film connecting to the upper channel wall), these sharply curved regions occur at vertices away from channel walls. By contrast, for films connecting to the upper channel wall sharp curvature occurs at the channel wall itself. We do not however need to resolve these sharply curved regions in what follows.

To obtain the geometrically invariant (i.e. flat film) state for an N-bubble staircase, we need to work from the downstream end of the structure to the upstream end, computing the various P_J, $\phi_{J-1,J}$, $\phi_{J-1,J+1}$ and $\phi_{J,J+1}$ values as we go. This then is what is achieved in the sections to follow.

(c) Analysing downstream end and implications for bubble pressures

We start by showing a detailed view of the downstream end of the structure (figure 3). We set the pressure to be zero outside the staircase structure at its downstream end. Hence $P_{N+1} = 0$. The film at the far downstream end is designated film $N, N+1$. It needs to meet the upper channel wall at right angles. Hence, the tangent to that film is vertical, and thus $\phi_{N,N+1} = 0$. This immediately tells us via equation (4.3) that the pressure P_N is unity. Film $N-1, N+1$ meanwhile needs to meet the lower channel wall at right angles. Hence, the pressure P_{N-1} is also unity.

It follows that there is no pressure difference between bubbles $N-1$ and N. The film orientation angle $\phi_{N-1,N}$ therefore satisfies $\phi_{N-1,N} = \pi/2$. Note that this indicates (figure 3) that film $N-1, N$ is parallel to the channel walls, and hence that film can never reach either of the channel walls (assuming it is flat, which must be the case for arbitrarily high driving pressure; specifically, what is taken to be arbitrarily high here is the pressure prior to the normalization described in §4a). This incidentally is sufficient to demonstrate that a simple lens (see figure S3 in the electronic supplementary material) cannot survive out to arbitrarily high pressures [45]: for a simple lens ($N = 1$), film $N-1, N$ becomes the same as film $0, 1$ and this needs to reach the upper channel wall. To do that, the film must curve (as figure S3 shows) and this is incompatible with a high-pressure limit that would require it to become asymptotically flat. For odd N, we need therefore to have $N \geq 3$ (see e.g. figure 1) in order to obtain the sort of flat film structures to be analysed here.

Turning to some of the other films shown in figure 3, there is formally a requirement for film $N, N+1$ (separating bubble N from the outside of the structure) and film $N-1, N+1$ (separating bubble $N-1$ from the outside of the structure) to meet at an angle of $2\pi/3$. In figure 3 it appears as though this is not happening. However, films $N, N+1$ and $N-1, N+1$ are allowed to curve sharply within an arbitrarily small region at their upstream ends. Of course because the asymptotically flat sections of the two films are oriented vertically rather than obliquely, it is not immediately apparent in figure 3 which is the 'upstream' end of each film in question. However

arguments presented in the literature [41,45] (see also the sketch in figure S4*a* in the electronic supplementary material) show that the upstream ends for both of these two films are the ends away from the channel wall, where the films meet at vertex N. That then is how the correct meeting angle can be attained, even though the angle itself is not resolved in figure 3.

Note moreover that film $N-1, N+1$ in particular is an example of a film that connects the lower channel wall (which it meets at right angles) to an odd-numbered vertex N (at which the film at its upstream end curves sharply). In fact, it turns out that all films which connect the lower channel wall to odd-numbered vertices obey the same condition: i.e. provided J is odd, they all have $\phi_{J-1,J+1}=0$ on their flat sections, and so the flat sections all meet the channel wall at right angles. In other words, as figure 2 indicates, all films connecting to the lower channel are vertical, as §4b already described.

According to equation (4.3) this means that moving upstream from each even-numbered bubble to the next, the pressure increments by unity. Hence

$$P_J = \frac{(N+1-J)}{2} \quad \text{for even } J. \tag{4.4}$$

Note in particular that the pressure outside the structure at the far upstream end satisfies $P_0 = (N+1)/2$.

It follows that $P_0^{-1} = 2/(N+1)$. This quantity P_0^{-1} is important: because of the way pressures have been normalized (see equation (4.2)), P_0^{-1} is a dimensionless measure of the mobility (mobility having been already identified within the Introduction as being an important quantity). Provided the staircase topology is preserved, we infer that mobility depends only on topology, but is otherwise independent of geometry (i.e. it is independent of bubble sizes). Moreover, the greater the number of bubbles that are present in the staircase, the lower the mobility becomes. We reiterate that mobility can be computed here even without knowing other geometrical details (e.g. bubble sizes or film lengths). This is a feature of the high-imposed pressure limit with flat films. Away from the high-pressure limit those other geometrical details can still affect mobility [41].

In view of equation (4.4), what remains to be calculated are the pressures P_J in the odd-numbered bubbles, the orientation angles $\phi_{J-1,J+1}$ in films connecting to the upper channel wall (for odd J), and the orientation angles $\phi_{J-1,J}$ and $\phi_{J,J+1}$ in films that zigzag across the structure from vertex to vertex. These quantities are calculated by alternating between even- and odd-numbered vertices as follows.

(d) Analysing even-numbered vertices

Consider an even-numbered vertex J: one film arrives at the vertex from the right, two films leave to the left (figure 4). It is supposed that the orientation angle $\phi_{J,J+1}$ of the film arriving from the right is known. This particular orientation angle is measured from the vertical, albeit not at vertex J but rather at the next vertex to the right (vertex $J+1$). Nonetheless, this orientation angle $\phi_{J,J+1}$ tells us nothing *a priori* about how vertex J itself is oriented. This is because film $J, J+1$ can in principle curve sharply near its upstream end as it arrives at vertex J. Whether or not it does curve sharply in this fashion is a point to be considered later.

More usefully for determining the configuration of vertex J, it is supposed that the pressure P_{J+1} of odd-numbered bubble $J+1$ is already known. The pressure P_J of even-numbered bubble J is also known (see equation (4.4)). Unknowns at vertex J, therefore are the pressure P_{J-1} and the orientation angles $\phi_{J-1,J+1}$ and $\phi_{J-1,J}$ of the films leaving the vertex to the left. These orientation angles are measured from the vertical (at vertex J).

Three equations are needed to solve for these three unknowns. These equations are

$$P_{J-1} - P_{J+1} = \cos(\phi_{J-1,J+1}), \tag{4.5}$$

which follows from equation (4.3),

$$P_{J-1} - P_J = -\cos(\phi_{J-1,J}), \tag{4.6}$$

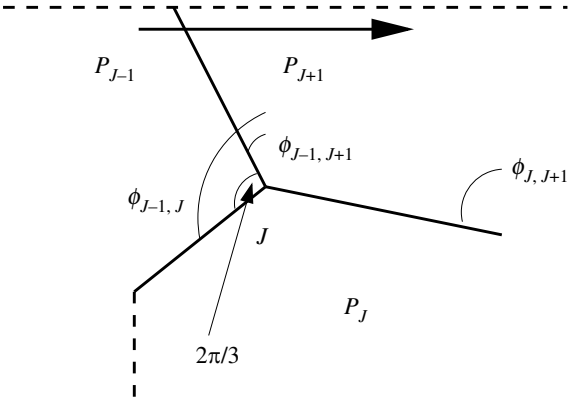

Figure 4. Configuration at an even-numbered vertex. Note the $2\pi/3$ angle between film $J-1, J+1$ and film $J-1, J$.

which also follows from equation (4.3), and

$$\phi_{J-1,J} = \phi_{J-1,J+1} + \frac{2\pi}{3}. \tag{4.7}$$

This follows from the requirement that films $J-1, J$ and $J-1, J+1$ meet an angle $2\pi/3$ at their downstream ends. Note the negative sign included on the right-hand side of equation (4.6): this is required because $\cos(\phi_{J-1,J})$ is a negative quantity.

Upon eliminating variables, the above equations lead to

$$\cos(\phi_{J-1,J+1}) + P_{J+1} + \cos\left(\phi_{J-1,J+1} + \frac{2\pi}{3}\right) - P_J = 0. \tag{4.8}$$

This is a nonlinear equation to solve for the single unknown $\phi_{J-1,J+1}$. As we will see, it turns out that we are interested in solutions for $\phi_{J-1,J+1}$ between 0 and $\pi/6$. Over this domain, $\cos(\phi_{J-1,J+1}) + \cos(\phi_{J-1,J+1} + 2\pi/3)$ is found to be a monotonic function of $\phi_{J-1,J+1}$. This means that if we find a solution for $\phi_{J-1,J+1}$ it will be unique (a point we return to in §4f). The above equation does not contradict the notion that film $J-1, J+1$ formally needs to meet the upper channel wall at right angles: the film does this by curving sharply at its upstream end where it meets the wall. However, equation (4.8) is only concerned with determining the value of $\phi_{J-1,J+1}$ on the asymptotically flat section of the film away from the upstream end. Film $J-1, J$ also curves sharply at its upstream end. This occurs at an odd-numbered vertex, as will be analysed next.

(e) Analysing odd-numbered vertices

Consider now an odd-numbered vertex J (figure 5). Two films (denoted here $J, J+1$ and $J-1, J+1$) now arrive from the right, and only one leaves towards the left. The orientation angle of film $J, J+1$ is $\phi_{J,J+1}$ (measured from the vertical albeit now at vertex $J+1$ not at vertex J). Film $J-1, J+1$ meanwhile as drawn is oriented vertically (and hence formally $\phi_{J-1,J+1} = 0$). Both of these films are however liable to reorient by curving sharply at their upstream ends: they reorient in order to meet film $J-1, J$ at angles of $2\pi/3$. Indeed it is owing to this reorientation that film $J-1, J+1$, which is otherwise vertical as has been mentioned, does in fact arrive from the right. Unfortunately all this means that knowing the values of $\phi_{J,J+1}$ and $\phi_{J-1,J+1}$ on the flat sections of these films furnishes no information about the orientation angle $\phi_{J-1,J}$.

More usefully though it can be assumed that the pressure P_J in odd-numbered bubble J is already known. Also, the pressures in all even-numbered bubbles are known (see equation (4.4)) and hence pressure P_{J-1} in particular is known. Equation (4.3) now implies

$$P_{J-1} - P_J = \cos(\phi_{J-1,J}) \quad \text{for odd } J, \tag{4.9}$$

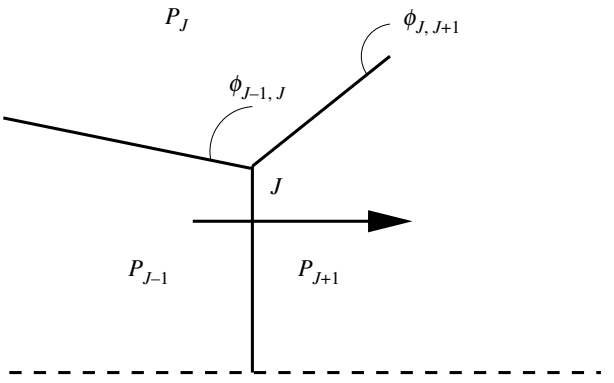

Figure 5. Configuration at an odd-numbered vertex.

which is rearranged to give a film orientation angle

$$\phi_{J-1,J} = \arccos(P_{J-1} - P_J). \tag{4.10}$$

Taken together equations (4.5)–(4.8) and (4.10) can be used to work from downstream to upstream, alternating between even- and odd-numbered vertices. However, solving the system remains awkward because equation (4.8) as written involves solving a nonlinear system, rather than having a closed-form expression for $\phi_{J-1,J+1}$ for even J. Surprisingly however such an expression exists, as is described next.

(f) Solving at even-numbered vertices

Now that we have information about both even-numbered and odd-numbered vertices, it is possible to use all this information to analyse even-numbered vertices in more detail. Indeed, for even J, it is possible to find a solution assuming that film orientation angles are related via

$$\phi_{J-1,J+1} = \phi_{J,J+1} - \frac{\pi}{3}, \tag{4.11}$$

and hence via equation (4.7)

$$\phi_{J-1,J} = \phi_{J,J+1} + \frac{\pi}{3}. \tag{4.12}$$

A proof that this then provides a solution is given in section S3. Mathematically working with equations (4.11)–(4.12) is far simpler than trying to solve the nonlinear equation (4.8) that is presented in §4d. Recall also from §4d that, once we find a $\phi_{J-1,J+1}$ value that is able to satisfy equation (4.8), we know it is unique, at least over the solution domain of interest here.

What all of this now means geometrically (see the electronic supplementary material, section S3) is that (for even J) film $J, J+1$ (which zigzags from vertex $J+1$ to vertex J) manages to meet vertex J without requiring any sharp curvature at its upstream end. Another way of interpreting this geometrically is that, at even-numbered vertices, the straight sections of all three films at the vertex meet at $2\pi/3$ angles in line with Plateau's laws. However, the configuration of the three films is rotated (by an amount $\phi_{J-1,J+1}$) relative to an infinite staircase. Moreover, this rotation amount $\phi_{J-1,J+1}$ varies from one even-numbered vertex to nearby even-numbered vertices (see figure S5 in the electronic supplementary material). As a result of the changing rotation amount, it is necessary to introduce a sharp curvature at the upstream end of certain films to ensure that elsewhere in the structure films meet at the correct angles. Indeed (again see the electronic supplementary material, figure S5), zigzag films leaving even-numbered vertices in the upstream direction need sharp curvature at their upstream ends (where they meet *odd*-numbered vertices).

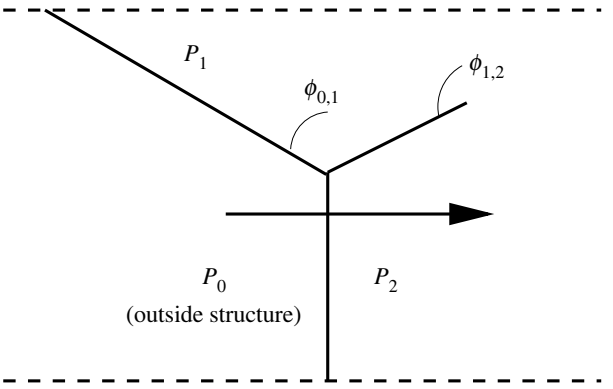

Figure 6. Configuration at the upstream end of the staircase.

We can now work upstream to compute the structure by iterating straightforwardly between equations (4.11)–(4.12) and equation (4.10) to obtain orientation angles for the entire staircase merely performing function evaluations, without the need to solve any nonlinear equations. As we work upstream, equations (4.4)–(4.6) also allow us to obtain bubble pressures. When J is even, equation (4.4) gives the value of P_J, whereas formulae for pressure P_{J-1} follow from either of equations (4.5)–(4.6) (these formulae are equivalent, provided equations (4.11)–(4.12) are satisfied).

Note, in particular, the situation at the furthest downstream even-numbered vertex (namely vertex $N-1$). Since we already know $\phi_{N-1,N}=\pi/2$, it follows that (for the film connecting vertex $N-1$ to the upper channel wall) the orientation angle is $\phi_{N-2,N}=\pi/6$ and (for the film zigzagging to the next vertex) the orientation angle is $\phi_{N-2,N-1}=5\pi/6$. Note also that $P_{N-2}=1+(\sqrt{3}/2)$, which follows from equation (4.5). These are results that are already known [45] from the three-bubble structure (figure 1), in which case there is only a single even-numbered vertex. However, they carry over to the analysis of the furthest downstream even-numbered vertex for any N.

The question now arises as to what happens far upstream as the number of bubbles N increases: the expectation for an even-numbered vertex J is that film $J-1, J+1$ (which connects to the upper channel wall) is that $\phi_{J-1,J+1}$ would decay below $\pi/6$ and eventually this film will approach vertical as in an infinite staircase. Working through the structure though from downstream to upstream alternating between even- and odd-numbered vertices, eventually we reach vertex 1 (the leftmost vertex), which is considered next.

(g) Analysing upstream end

Mathematically, the formula for determining the film orientation angle at vertex 1 is no different from equation (4.10) for any arbitrary odd-numbered vertex. The geometry is however slightly different in that film 0, 1 now extends all the way up to the upper channel wall (figure 6).

To start with it is instructive to consider the three-bubble structure, such that bubble 1 is the same as bubble $N-2$ (and the pressure P_{N-2} is given in §4f already). The pressure P_{N-3} meanwhile can be obtained from equation (4.4): for the three-bubble structure of course, this is simply the pressure outside the structure at the upstream end. It follows that the orientation angle of the backmost film denoted $\phi_{0,1}$ has, for the three-bubble structure, a value $\arccos(1-(\sqrt{3}/2))$ (around $0.4572\,\pi$, a result already known from the literature [45]; see also figure 1).

This same film orientation however applies to film $N-3, N-2$ for a general N. Observe that the orientation angle $\phi_{N-3,N-2}$ is smaller than $\phi_{N-1,N}$ (the value of $\phi_{N-1,N}$ is $\pi/2$, as per §4c). However, $\phi_{N-3,N-2}$ still exceeds $\pi/3$, which is the analogous orientation angle in an infinite staircase. As N increases though, it is expected that the orientation angle of the backmost film $\phi_{0,1}$ should become closer to $\pi/3$. How systems behave in the limit of very large N is considered

next (noting however that N is assumed odd here; even values of N are however discussed in the electronic supplementary material, section S5).

5. Behaviour for an arbitrarily long bubble staircase

In this section, we present limiting behaviour for an arbitrarily long staircase (§5a) and also the asymptotic approach to that limiting behaviour (§5b).

(a) Limiting behaviour for a long staircase

Arbitrarily far back from the downstream end of an arbitrarily long staircase, equations (4.5)–(4.12) exhibit a limiting solution, as can easily be seen by inspection. For an even-numbered vertex J (with J much smaller than N), we find $\phi_{J-1,J+1} \to 0$, $\phi_{J-1,J} \to 2\pi/3$. It also follows that $\phi_{J,J+1} \to \pi/3$ (albeit this orientation angle would be measured at vertex $J+1$ not at vertex J). The orientation of all the films in this region is now the same as in an infinite staircase. In other words, films connected to the upper channel wall are vertical, and the remaining films zigzag from vertex to vertex satisfying Plateau's Laws. Note that all films connected to the lower channel wall are vertical (regardless of where they are in the structure). Films connected to the upper channel wall only become vertical far upstream.

In addition to limiting behaviour for film orientation angles, it is also possible to obtain the limiting behaviour for pressures. Considering an even-numbered vertex J far upstream, there is a unit change in pressure from odd-numbered bubble $J+1$ to odd-numbered bubble $J-1$ (as equation (4.5) now implies). However (as equation (4.6) with $\phi_{J-1,J} \to 2\pi/3$ shows), there is only a change of half a unit in pressure from even-numbered bubble J to odd-numbered bubble $J \pm 1$. This means that equation (4.4), which applies for even-numbered bubbles throughout the entire structure, is also valid for odd-numbered bubbles sufficiently far upstream. In other words, bubble pressure satisfies

$$P_J \to \frac{(N+1-J)}{2} \quad \text{for odd } J \text{ far upstream.} \tag{5.1}$$

Coupled with equation (4.4), this does indeed give a difference of half a unit of pressure between adjacent odd-numbered and even-numbered bubbles far upstream. Note that at the downstream end of the structure (see §4c), odd-numbered bubble N has the same pressure as even-numbered bubble $N-1$, and equation (5.1) does not apply. As we move upstream though, the pressure in odd-numbered bubble J ceases to be the same as that in even-numbered bubble $J-1$, and eventually falls half a unit below.

(b) Asymptotic behaviour for a long staircase

The analysis in §5a gives limiting behaviour of the staircase structure far upstream, but not how quickly that limiting behaviour is approached. This can however be determined.

Suppose we consider an even-numbered vertex J (as per figure 4), and bubbles $J-1$, J and $J+1$ around it. Suppose moreover that $\Pi_{J\pm1}$ represents a deviation of bubble pressure from the prediction of equation (5.1). In other words, $P_{J\pm1}$ is given by the prediction of equation (5.1) plus a correction $\Pi_{J\pm1}$ remembering here that J is even, so that $J \pm 1$ is odd. Assuming that $\Pi_{J\pm1}$ and $\phi_{J-1,J+1}$ are small parameters, equation (4.6) coupled with equations (4.11)–(4.12) Taylor expands to

$$\Pi_{J-1} \approx \sin\left(\frac{2\pi}{3}\right)\phi_{J-1,J+1} = \sqrt{3}\phi_{J-1,J+1}/2. \tag{5.2}$$

Specifically what we have done is to use equation (4.4), equation (5.1) and the definition of Π_{J-1}, which are all substituted into the left-hand side of equation (4.6). Meanwhile a difference between equation (4.11) and (4.12) is taken to express $\phi_{J-1,J}$ in terms of $\phi_{J-1,J+1}$. This is substituted into

the right-hand side of equation (4.6), which is then Taylor expanded to first order in $\phi_{J-1,J+1}$. Meanwhile equation (4.5) Taylor expands to

$$\Pi_{J-1} - \Pi_{J+1} \approx -\phi_{J-1,J+1}^2/2. \tag{5.3}$$

On the left-hand side of equation (4.5), we have used equation (5.1) and the definition of $\Pi_{J\pm1}$. On the right-hand side, we have Taylor expanded to second order in $\phi_{J-1,J+1}$, as the first-order term vanishes here.

Equation (5.2) indicates that the pressure deviation is proportional to the angle by which the film joining to the upper channel wall deviates from the vertical. Equation (5.3) indicates the amount by which the pressure deviation decays from one bubble to the next is small being only second order in angle, i.e. the resulting decay is rather slow.

Analysis of equations (5.2)–(5.3) is given in the electronic supplementary material, section S4. It is found that

$$\phi_{J-1,J+1} \sim \frac{2\sqrt{3}}{(N+1-J)}, \tag{5.4}$$

for even J. We also deduce

$$\Pi_J \sim \frac{3}{(N+1-J)}, \tag{5.5}$$

albeit applicable now for odd J. In what follows, these asymptotic predictions will be compared with computed values.

6. Results

In this results section, we first consider bubble pressures (§6a) and then we consider film orientations (§6b). Throughout, data have been obtained via the procedure already described in §4f, i.e. working from downstream to upstream iterating between equations (4.11)–(4.12) and equation (4.10), with pressures given by equations (4.4)–(4.6).

(a) Results: bubble pressures

Figure 7*a* presents the bubble pressures P_J as a function of $N+1-J$. Observe that the quantity $N+1-J$ here is the bubble number but counting from downstream to upstream (not upstream to downstream as we conventionally do). Values of P_J depend only on $N+1-J$, not on N and J individually.

Note that P_J values for even J all fall on a straight line (see equation (4.4)). For odd-numbered J, values of P_J start off close to P_{J-1}, at least when $N+1-J$ is relatively small. However as $N+1-J$ increases, values of P_J with odd-numbered J gradually move midway between P_{J-1} and P_{J+1}, i.e. they migrate towards the prediction of equation (5.1), which gives the same straight line as mentioned previously.

Figure 7*b* shows how Π_J (i.e. the deviation of pressure P_J from equation (5.1)) decays as a function of $N+1-J$ albeit plotting only for odd values of J (as the deviation vanishes in the case of even J). The asymptotic formula given by equation (5.5) is also plotted here. Visually, this agrees reasonably well with the computed Π_J for $N+1-J$ values greater than roughly 50, and the agreement is easy to check on a log-log plot (see figure S7*a* in the electronic supplementary material). Note also the slow decay of Π_J. For instance, when $J=N$, the value of Π_J is 1/2. However, for Π_J to fall by an order of magnitude relative to this, equation (5.5) suggests $N+1-J$ needs to be greater than around 60. To achieve this anywhere at all in the staircase, we would need N values of around 60 or greater (remembering also that N is assumed odd here).

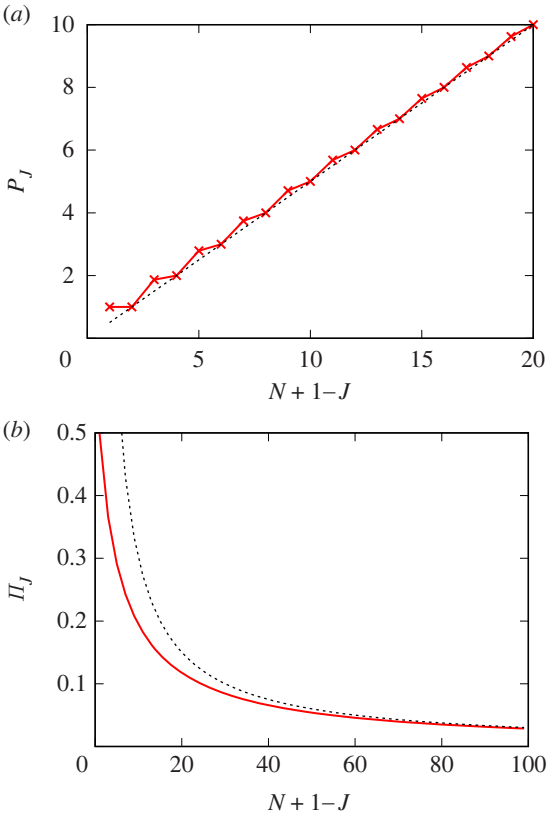

Figure 7. (*a*) Pressure P_J in bubble J versus $N+1-J$ in an N-bubble staircase. Here, J represents the bubble number counting from upstream to downstream, whereas $N+1-J$ represents the bubble number counting from downstream to upstream. The dashed line shows a formula that is applicable for even-numbered bubbles (anywhere in the staircase) and for odd-numbered bubbles (in the limit far upstream only). (*b*) Pressure deviation Π_J (relative to the far upstream limiting formula, shown here for odd-numbered bubbles only) versus $N+1-J$. The dashed line shows an asymptotic approximation to Π_J.

(b) Results: film orientations

Figure 8 plots the orientation angle $\phi_{J-1,J+1}$ as a function of $N+1-J$. Only even values of J are considered (since $\phi_{J-1,J+1}$ vanishes when J is odd). Clearly, in figure 8, the value of $\phi_{J-1,J+1}$ decays with increasing $N+1-J$. Values of $\phi_{J-1,J}$ and $\phi_{J,J+1}$ can now also be deduced easily from equations (4.7) and (4.11) but values are not plotted here, since equations (4.7) and (4.11) are already very straightforward.

The asymptotic formula given by equation (5.4) is also shown in figure 8 and visually it agrees with the computed orientation angle $\phi_{J-1,J+1}$ for $N+J-1$ values greater than about 50 (see also the log-log plot in figure S7*b* in the electronic supplementary material). Again, a slow decay is seen here. For instance, when $J=N-1$, the value of $\phi_{J-1,J+1}$ is $\pi/6$. However, to fall to an order of magnitude below this, equation (5.4) implies $N+1-J$ would need to exceed around 66. To achieve this anywhere at all in the staircase, N would likewise need to exceed around 66. This is comparable with the findings of §6a, which suggested N values of around 60 or more for discrepancies relative to an infinite staircase to decay by an order of magnitude (remembering also here that the infinite staircase has $\phi_{J-1,J+1}$ vanishing). Hence film orientations (and bubble pressures likewise) retain a long 'memory' even quite some way from the downstream end of the staircase that they are part of a finite staircase rather than an infinite one. This at least is the case in the limit considered here with high imposed driving pressures. Overall conclusions and the outlook for comparing finite staircases with infinite staircases are discussed next.

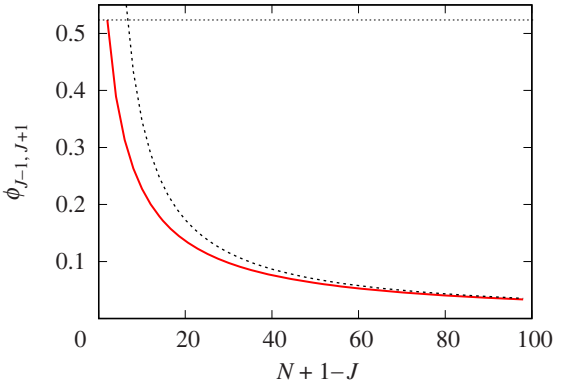

Figure 8. Film orientation angle $\phi_{J-1,J+1}$ (for films connecting to the upper channel wall, for even-numbered J only) versus $N+1-J$. The dashed line shows an asymptotic approximation to $\phi_{J-1,J+1}$. The horizontal dotted line shows the constant value $\phi_{N-2,N} \equiv \pi/6$ (i.e. the orientation angle obtained towards the downstream end).

7. Conclusion and outlook

The configuration of N bubbles arranged in a Hele–Shaw channel in a staircase geometry has been considered. The gap thickness of the Hele–Shaw channel is assumed much smaller than the channel width, so the staircase can be treated as two-dimensional. To impose topological asymmetry, it is assumed that N is odd, so that $(N+1)/2$ bubbles attach to the upper channel wall, whereas $(N-1)/2$ bubbles attach to the lower channel wall. Equivalently, $(N+3)/2$ films connect to the upper channel wall, and $(N+1)/2$ films connect to the lower channel wall. The focus here has been on trying to understand systems with large but finite N, building on prior work with much smaller N values (e.g. $N=1$ as considered in one prior study [41] or $N=3$ as considered by other studies [45–47]).

Constraints on film meeting angles are imposed: Plateau's Laws apply wherever three films meet and (subject to Hele–Shaw gap thickness being much smaller than channel width) films meet channel walls at right angles. In the limit considered here (a large imposed driving pressure or equivalently rapid motion of bubbles along the channel), foam films become asymptotically flat. Thus, if films curve at all, they curve only at their upstream ends, and curvature is sharp there. As a consequence, even though the aforementioned constraints on film meeting angles are still satisfied, by looking solely at the asymptotically flat sections of the films, those rules might appear to be violated.

The configurations of the asymptotically flat sections of the films can nonetheless be determined independently of the curved sections. Film configurations in a finite staircase of N bubbles differ from those in an infinite staircase. In particular, films that connect to the upper channel wall, and which separate even-numbered bubbles, are rotated with respect to the analogous films in an infinite staircase. Moving upstream, these films gradually align with the orientation in an infinite staircase. However, the process is gradual. We would need as many as 60 or so bubbles in a finite staircase for the discrepancy in orientation angle towards the upstream end to fall by an order of magnitude compared with what it is at the downstream end. In other words, up to 60 or so bubbles back from the downstream end retain a 'memory' of being in a finite staircase, at least when the staircase is driven at high imposed pressure. That said, if the number of bubbles is far in excess of 60, then film orientations over most of the staircase (away from the downstream end) would be close to the film orientations for the infinite staircase.

The above-mentioned memory effects could be useful in practice in microfluidic applications. For instance, in figure 2, the zigzag films that separate odd-numbered bubbles J (e.g. $J=N-2$ or $J=N-4$) from even-numbered neighbours $J\pm1$ are not oriented symmetrically. It is likely that these asymmetric orientations are reflected also in asymmetric film lengths (although we

have not actually computed any film lengths in the present work). In figure 2, for instance, the film separating odd-numbered bubble J from even-numbered bubble $J+1$ is sketched as possibly being shorter than the film separating that same bubble J from even-numbered bubble $J-1$. If mass transfer is taking place from odd-numbered bubble J to its even-numbered neighbours, then as drawn in figure 2 at least, less mass will be transferred to bubble $J+1$ than to bubble $J-1$. Clearly, however, we can only make definite predictions about this once we have computations of film lengths, a point we return to mention shortly.

As well as computing film orientation angles, it is also possible to compute bubble pressures. The pressures in odd-numbered bubbles lie somewhere between pressures in immediately adjacent even-numbered bubbles downstream and upstream of them. However, they tend to be closer to the pressures on the immediately upstream side rather than the downstream side. Very far towards the upstream end of a staircase with a large number of bubbles, pressures in odd-numbered bubbles approach halfway between those in adjacent even-numbered bubbles. However, as also happened with film orientations, the approach here is gradual.

One notable feature of the high driving pressure limit considered here is that film orientations and bubble pressures can be determined independently of the bubble sizes. All staircases that have been analysed here, regardless of the bubble sizes within them, then have the same set of film orientations and the same set of bubble pressures. This means that (in line with findings in the literature [47]) the mobility of the structure depends only on the number of bubbles present, and how they are arranged topologically provided the topology remains fixed. Mobility does not depend on other geometrical aspects such as bubble sizes or film lengths, at least mobility does not depend on those aspects in the limit considered here assuming high imposed driving pressures. Having a simple way to determine mobility of various bubble structures might be useful in practice. For instance, the literature has found [47] that the three-bubble system tends to transform topologically so as to select bubble arrangements with lower mobility than other competing topological arrangements, although whether that also happens for N bubbles is unknown.

Of course, in order to compute the N-bubble staircase structure definitively, it is still necessary to fix bubble sizes and determine the associated film lengths: this aspect is left for further work. The outlook here is that not all choices of bubble size will admit a structure with the desired topology for the set of film orientations determined here. As happened in the three-bubble case, there is likely to be a set of minimum bubble areas below which the target structure will not even exist [45,46]. However, that set of minimum areas might depend on the number of bubbles present. There is no minimum area for an infinite staircase for instance.

Ultimately, it is desired to know to what extent a finite staircase (or at least parts of a staircase) might start to approach a configuration geometrically similar to an equivalent infinite staircase. In the high driving pressure limit, a necessary condition for this to happen is for the film orientations in the finite staircase to match those in the infinite case. Clearly, even to approach a condition like that, we need large values of N, around 60 or so as suggested above.

Although a necessary condition for the finite and infinite staircases to become close, this is not however sufficient. Instead, at the far upstream end of the structure, geometrically the system still differs from the infinite staircase. As figure 2 and figure 6 both show, in any finite staircase, the obliquely oriented backmost film (denoted film $0,1$) upon leaving the backmost vertex (denoted vertex 1) needs to be long enough to extend all the way up to the upper channel wall. In the infinite staircase however, obliquely oriented zigzag films tend to be shorter, since they never reach channel walls. Instead, they always terminate in vertical films, and it is then those vertical films that connect to the upper and lower channel walls. Hence at the upstream end of a staircase with a large but finite number of bubbles, there must be a geometrical difference from an infinite staircase in terms of film lengths, even if film orientations themselves differ little. This then makes it yet more important as part of the outlook for further work, as has been mentioned, to compute structures geometrically in terms of bubble sizes and film lengths.

The only situation in which the configuration at the backmost film in figure 6 represents a small perturbation geometrically from an infinite staircase is the scenario in which zigzag films in the infinite staircase are long and vertical films are short. This gives an infinite staircase with bubbles of comparatively large area (see also figure S2*b* in the electronic supplementary material). Starting from the far upstream end of a large but finite bubble staircase itself comprised of bubbles of large area, and then moving just a few bubbles downstream, the hope is that a structure akin to an infinite staircase might be reached, not just in terms of film orientations but in terms of film lengths also.

A final comment we make is that all we have achieved here is to determine information about how a geometrically invariant state for an N-bubble structure must be configured, assuming the limit of high imposed driving pressures is attained. It is possible that even though a geometrically invariant state can exist in principle, it might not necessarily be realized in practice: instead, as very often happened with the three-bubble structure [45,46], the staircase might break in various ways even before the high-pressure limit is reached. On the other hand, the infinite staircase is expected to be stable, migrating as it does without deforming. Intuitively, therefore, the larger the value of N that is selected for a finite staircase, the more likely it should be that a geometrically invariant state is indeed attained when increasing pressures are imposed, which can be done either gradually [45] or suddenly [46]. However, we have still not demonstrated whether such intuition is correct. That said, having information about how a geometrically invariant state needs to be configured (the contribution of the present work), is an essential step towards testing whether such a configuration is actually attained in practice. The first step is determining film orientations, as has been done here. The next step (as already alluded to above) is constructing a configuration with bubbles of required target areas respecting those film orientations. After that is done, we can test the dynamic stability of the configuration to perturbations, to ascertain whether it might be realizable.

Data accessibility. All results presented here are reproducible by procedures detailed in the article and the electronic supplementary material. Raw data analysed are also provided in section S6 of the electronic supplementary material [58].

Declaration of AI use. We have not used AI-assisted technologies in creating this article.

Authors' contributions. P.G.: conceptualization, formal analysis, funding acquisition, investigation, methodology, software, supervision, writing—original draft, writing—review and editing; C.T.-U.: conceptualization, formal analysis, funding acquisition, investigation, methodology, software, writing—original draft, writing—review and editing; J.H.: formal analysis, supervision, writing—review and editing.

All authors gave final approval for publication and agreed to be held accountable for the work performed therein.

Conflict of interest declaration. We declare we have no competing interests.

Funding. P.G. acknowledges support from EPSRC grant no. EP/V002937/1. C.T.-U. acknowledges support from Centro de Investigación, Innovación y Creación UCT (CIIC-UCT).

Acknowledgements. C.T.-U. acknowledges S. Cox, D. Vitasari, E. Mas-Hernández and G. Montecinos for hosting research visits during which useful discussions took place.

References

1. Johnson P, Starov V, Trybala A. 2022 Foam flow through porous media. *Curr. Opin. Colloid Interface Sci.* **58**, 101555. (doi:10.1016/j.cocis.2021.101555)
2. Drenckhan W, Cox SJ, Delaney G, Holste H, Weaire D, Kern N. 2005 Rheology of ordered foams: on the way to discrete microfluidics. *Colloids Surf. A* **263**, 52–64. (doi:10.1016/j.colsurfa.2005.01.005)
3. Jia X, Mowatt G, Burr JM, Cassar K, Cook J, Fraser C. 2007 Systematic review of foam sclerotherapy for varicose veins. *Br. J. Surg.* **94**, 925–936. (doi:10.1002/bjs.5891)
4. Kotb MM, Shakiban HK, Sawaby AF. 2013 Foam treatment for varicose veins: efficacy and safety. *Alexandria J. Med.* **49**, 249–253. (doi:10.1016/j.ajme.2012.11.003)
5. Rossen WR. 1996 Foams in enhanced oil recovery. In *Foams: theory, measurements and applications* (eds RK Prud'homme, SA Khan), Surfactant Science Series, pp. 99–187. New York, NY: Marcel Dekker.

6. Shan D, Rossen WR. 2004 Optimal injection strategies for foam IOR. *SPE J.* **9**, 132–150. (doi:10.2118/88811-PA)
7. Li RF, Yan W, Liu S, Hirasaki GJ, Miller CA. 2010 Foam mobility control for surfactant enhanced oil recovery. *SPE J.* **15**, 928–942. (doi:10.2118/113910-PA)
8. Farajzadeh R, Andrianov A, Krastev R, Hirasaki GJ, Rossen WR. 2012 Foam-oil interaction in porous media: implications for foam assisted enhanced oil recovery. *Adv. Colloid Interface Sci.* **183–184**, 1–13. (doi:10.1016/j.cis.2012.07.002)
9. Dong P *et al.* 2018 Low-IFT foaming system for enhanced oil recovery in highly heterogeneous/fractured oil-wet carbonate reservoirs. *SPE J.* **23**, 2243–2259. (doi:10.2118/184569-PA)
10. Føyen T, Brattekås B, Fernø MA, Barrabino A, Holt T. 2020 Increased CO_2 storage capacity using CO_2-foam. *Int. J. Greenhouse Gas Control* **96**, 103016. (doi:10.1016/j.ijggc.2020.103016)
11. Rossen WR, Farajzadeh R, Hirasaki GJ, Amirmoshiri M. 2022 Potential and challenges of foam-assisted CO_2 sequestration. In *SPE Improved Oil Recovery Conference, Virtual, 25th–29th April*.
12. Hirasaki GJ, Miller CA, Szafranski R, Lawson JB, Akiya N. 1997 Surfactant/foam process for aquifer remediation. In *SPE Annual Technical Conference, San Antonio, TX, 18th–21st February*.
13. Hirasaki GJ, Miller CA, Szafranski R, Tanzil D, Lawson JB, Meinardus H, Jin M, Londergan JT, Jackson RE, Pope GA, Wade WH. 1997 Field demonstration of the surfactant/foam process for aquifer remediation. In *SPE Annual Technical Conf. and Exhibition, San Antonio, TX, 5–8 October*.
14. Jeong SW, Corapcioglu MY. 2003 A micromodel analysis of factors influencing NAPL removal by surfactant foam flooding. *J. Contam. Hydrol.* **60**, 77–96. (doi:10.1016/s0169-7722(02)00054-2)
15. Mulligan CN, Eftekhari F. 2003 Remediation with surfactant foam of PCP-contaminated soil. *Eng. Geol.* **70**, 269–279. (doi:10.1016/S0013-7952(03)00095-4)
16. Wang S, Mulligan CN. 2004 An evaluation of surfactant foam technology in remediation of contaminated soil. *Chemosphere* **57**, 1079–1089. (doi:10.1016/j.chemosphere.2004.08.019)
17. Couto HJ, Massarani G, Biscaia EC, Santa-Anna GL. 2009 Remediation of sandy soils using surfactant solutions and foams. *J. Hazard. Mater.* **164**, 1325–1334. (doi:10.1016/j.jhazmat.2008.09.129)
18. Zhong L, Szecsody JE, Zhang F, Mattigod SV. 2010 Foam delivery of amendments for vadose zone remediation: propagation performance in unsaturated sediments. *Vadose Zone J.* **9**, 757–767. (doi:10.2136/vzj2010.0007)
19. Zhong L, Szecsody J, Oostrom M, Truex M, Shen X, Li X. 2011 Enhanced remedial amendment delivery to subsurface using shear thinning fluid and aqueous foam. *J. Hazard. Mater.* **191**, 249–257. (doi:10.1016/j.jhazmat.2011.04.074)
20. Longpré-Girard M, Martel R, Robert T, Lefebvre R, Lauzon JM. 2016 2D sandbox experiments of surfactant foams for mobility control and enhanced LNAPL recovery in layered soils. *J. Contam. Hydrol.* **193**, 63–73. (doi:10.1016/j.jconhyd.2016.09.001)
21. Bertin H, Del Campo Estrada E, Atteia O. 2017 Foam placement for soil remediation. *Environ. Chem.* **14**, 338–343. (doi:10.1071/EN17003)
22. Portois C, Boeije CS, Bertin HJ, Atteia O. 2018 Foam for environmental remediation: generation and blocking effect. *Transp. Porous Media* **124**, 787–801. (doi:10.1007/s11242-018-1097-z)
23. Farajzadeh R, Bertin H, Rossen WR. 2020 Editorial to the special issue: foam in porous media for petroleum and environmental engineering: experience sharing. *Transp. Porous Media* **131**, 1–3. (doi:10.1007/s11242-019-01329-4)
24. Longpré-Girard M, Martel R, Robert T, Lefebvre R, Lauzon JM, Thomson N. 2020 Surfactant foam selection for enhanced light non-aqueous phase liquids (LNAPL) recovery in contaminated aquifers. *Transp. Porous Media* **131**, 65–84. (doi:10.1007/s11242-019-01292-0)
25. Aranda R, Davarzani H, Colombano S, Laurent F, Bertin H. 2020 Experimental study of foam flow in highly permeable porous media for soil remediation. *Transp. Porous Media* **134**, 231–247. (doi:10.1007/s11242-020-01443-8)
26. Davarzani H, Aranda R, Colombano S, Laurent F, Bertin H. 2021 Experimental study of foam propagation and stability in highly permeable porous media under lateral water flow: diverting groundwater for application to soil remediation. *J. Contam. Hydrol.* **243**, 103917. (doi:10.1016/j.jconhyd.2021.103917)
27. Kovscek AR, Radke CJ. 1994 Fundamentals of foam transport in porous media. In *Foams: fundamentals and applications in the petroleum industry* (ed. LL Schramm), Advances in Chemistry, vol. 242, pp. 115–163. Washington, DC: American Chemical Society.

28. Gauglitz PA, Friedmann F, Kam SI, Rossen WR. 2002 Foam generation in homogeneous porous media. *Chem. Eng. Sci.* **57**, 4037–4052. (doi:10.1016/S0009-2509(02)00340-8)
29. Bretherton FP. 1961 The motion of long bubbles in tubes. *J. Fluid Mech.* **10**, 166–188. (doi:10.1017/S0022112061000160)
30. Park CW, Homsy GM. 1984 Two-phase displacement in Hele Shaw cells: theory. *J. Fluid Mech.* **139**, 291–308. (doi:10.1017/S0022112084000367)
31. Rossen WR. 1990 Theory of mobilization pressure gradient of flowing foams in porous media: I. Incompressible foam. *J. Colloid Interface Sci.* **136**, 1–16. (doi:10.1016/0021-9797(90)90074-X)
32. Cox SJ, Neethling S, Rossen WR, Schleifenbaum W, Schmidt-Wellenburg P, Cilliers JJ. 2004 A theory of the effective yield stress of foam in porous media: the motion of a soap film traversing a three-dimensional pore. *Colloids Surfaces A* **245**, 143–151. (doi:10.1016/j.colsurfa.2004.07.004)
33. Ferguson DJ, Cox SJ. 2013 The motion of a foam lamella traversing an idealised bi-conical pore with a rounded central region. *Colloids Surfaces A* **438**, 56–62. (doi:10.1016/j.colsurfa.2013.02.015)
34. Cantat I, Kern N, Delannay R. 2004 Dissipation in foam flowing through narrow channels. *Europhys. Lett.* **65**, 726–732. (doi:10.1209/epl/i2003-10169-0)
35. Cantat I, Delannay R. 2003 Dynamical transition induced by large bubbles in two-dimensional foam flows. *Phys. Rev. E* **67**, 031501. (doi:10.1103/PhysRevE.67.031501)
36. Kern N, Weaire D, Martin A, Hutzler S, Cox SJ. 2004 Two-dimensional viscous froth model for foam dynamics. *Phys. Rev. E* **70**, 041411. (doi:10.1103/PhysRevE.70.041411)
37. Cantat I, Delannay R. 2005 Dissipative flows of 2D foams. *Eur. Phys. J. E* **18**, 55–67. (doi:10.1140/epje/i2004-10154-5)
38. Cantat I, Poloni C, Delannay R. 2006 Experimental evidence of flow destabilization in a two-dimensional bidisperse foam. *Phys. Rev. E* **73**, 011505. (doi:10.1103/PhysRevE.73.011505)
39. Jones SA, Dollet B, Méheust Y, Cox SJ, Cantat I. 2013 Structure-dependent mobility of a dry aqueous foam flowing along two parallel channels. *Phys. Fluids* **25**, 063101 (doi:10.1063/1.4811178)
40. Géraud B, Jones SA, Cantat I, Dollet B, Méheust Y. 2016 The flow of a foam in a two-dimensional porous medium. *Water Resour. Res.* **52**, 773–790. (doi:10.1002/2015WR017936)
41. Green TE, Bramley A, Lue L, Grassia P. 2006 Viscous froth lens. *Phys. Rev. E* **74**, 051403. (doi:10.1103/PhysRevE.74.051403)
42. Cox SJ, Weaire D, Mishuris G. 2009 The viscous froth model: steady states and the high-velocity limit. *Proc. R. Soc. A* **465**, 2391–2405. (doi:10.1098/rspa.2009.0057)
43. Vitasari D, Cox S. 2017 A viscous froth model adapted to wet foams. *Colloids Surf. A* **534**, 8–15. (doi:10.1016/j.colsurfa.2017.04.064)
44. Vitasari D, Cox S, Grassia P, Rosario R. 2020 Effect of surfactant redistribution on the flow and stability of foam films. *Proc. R. Soc. A* **476**, 20190637. (doi:10.1098/rspa.2019.0637)
45. Torres-Ulloa C, Grassia P. 2022 Viscous froth model applied to the motion and topological transformations of two-dimensional bubbles in a channel: three-bubble case. *Proc. R. Soc. A* **478**, 20210642. (doi:10.1098/rspa.2021.0642)
46. Torres-Ulloa C, Grassia P. 2022 Viscous froth model applied to the dynamic simulation of bubbles flowing in a channel: three-bubble case. *Proc. R. Soc. A* **478**, 20220487. (doi:10.1098/rspa.2022.0487)
47. Torres-Ulloa C, Grassia P. 2023 Viscous froth model applied to multiple topological transformations of bubbles flowing in a channel: three-bubble case. *Proc. R. Soc. A* **479**, 20220785. (doi:10.1098/rspa.2022.0785)
48. Zhang H, Torres-Ulloa CA, An S, Brito-Parada PR, Neethling SJ, Wang Y. 2024 A comparative study of a viscous froth lens in two and three dimensions. *Phys. Fluids* **36**, 012106. (doi:10.1063/5.0174974)
49. Osei-Bonsu K, Shokri N, Grassia P. 2016 Fundamental investigation of foam flow in a liquid-filled Hele-Shaw cell. *J. Colloid Interface Sci.* **462**, 288–296. (doi:10.1016/j.jcis.2015.10.017)
50. Stewart PS, Hilgenfeldt S. 2023 Gas-liquid foam dynamics: from structural elements to continuum descriptions. *Annu. Rev. Fluid Mech.* **55**, 323–350. (doi:10.1146/annurev-fluid-032822-125417)
51. Grassia P, Montes-Atenas G, Lue L, Green TE. 2008 A foam film propagating in a confined geometry: analysis via the viscous froth model. *Eur. Phys. J. E* **25**, 39–49. (doi:10.1140/epje/i2007-10262-8)

52. Weaire D, Hutzler S. 1999 *The physics of foams*. Oxford, UK: Oxford University Press.
53. Cantat I, Cohen-Addad S, Elias F, Graner F, Höhler R, Pitois O, Rouyer F, Saint-Jalmes A. 2013 *Foams: structure and dynamics*. Oxford, UK: Oxford University Press.
54. Hinch EJ. 1991 *Perturbation methods*. Cambridge, UK: Cambridge University Press.
55. Saugey A, Drenckhan W, Weaire D. 2006 Wall slip of bubbles in foams. *Phys. Fluids* **18**, 053101. (doi:10.1063/1.2196912)
56. Dollet B, Cantat I. 2010 Deformation of soap films pushed through tubes at high velocity. *J. Fluid Mech.* **652**, 529–539. (doi:10.1017/S0022112010000935)
57. Grassia P, Mas-Hernández E, Shokri N, Cox SJ, Mishuris G, Rossen WR. 2014 Analysis of a model for foam improved oil recovery. *J. Fluid Mech.* **751**, 346–405. (doi:10.1017/jfm.2014.287)
58. Grassia P, Torres-Ulloa C, Hernández-Montelongo J. 2024 A cluster of *N*-bubbles driven along a channel at high imposed driving pressure: film orientations and bubble pressures. Figshare. (doi:10.6084/m9.figshare.c.7315701)